Nonlinear Chirp Mode Decomposition: A Variational Method

Shiqian Chen, Xingjian Dong, Zhike Peng, Wenming Zhang, *Member, IEEE*, and Guang Meng

***Abstract*—Variational mode decomposition (VMD), a recently introduced method for adaptive data analysis, has aroused much attention in various fields. However, the VMD is formulated based on the assumption of narrow-band property of the signal model. To analyze wide-band nonlinear chirp signals (NCSs), we present an alternative method called variational nonlinear chirp mode decomposition (VNCMD). The VNCMD is developed from the fact that a wideband NCS can be transformed to a narrow-band signal by using demodulation techniques. Our decomposition problem is, thus, formulated as an optimal demodulation problem, which is efficiently solved by the alternating direction method of multipliers. Our method can be viewed as a time–frequency filter bank, which concurrently extracts all the signal modes. Some simulated and real data examples are provided showing the effectiveness of the VNCMD in analyzing NCSs containing close or even crossed modes.**

***Index Terms*—Variational mode decomposition, nonlinear chirp signal, signal decomposition, alternating direction method of multipliers, time-frequency.**

I. Introduction

MANY everyday signals, such as those from human speech, animal sounds, radar systems and mechanical systems, usually display nonlinear and nonstationary characteristics [1]–[4]. Generally, these signals exhibit complicated time-varying amplitudes and frequencies and are often called nonlinear chirp signals (NCSs) [5]. The traditional spectral analysis methods only give global frequency information and thus cannot characterize time-varying frequency contents of NCSs. In addition, practical NCSs from physical measurements are typically composed of many nonlinear chirp modes (NCMs), which makes the analysis of such signals more challenging. To have a deep understanding of the signal properties, one needs first to extract each NCM from the signal data. In the past few decades, many methods have been developed to decompose NCSs. These methods achieve signal decompositions either in the time, frequency or time-frequency (TF) domains.

Most decomposition methods directly extract each signal mode in the time domain, among which the empirical mode decomposition (EMD) is the most well-known one [6]. The EMD is a fully data-driven method and can adaptively decompose a complicated NCS into some simple modes. Although the EMD is sensitive to noise and sampling, and lacks mathematical foundations, it has been widely applied in various fields [7]–[9]. Many efforts have also been made to improve the EMD by using optimization methods [10]–[12]. However, these methods only solve parts of the problems and some challenging issues still remain to be addressed. For instance, these EMD-based methods have poor resolution to separate close modes [13]. Another popular method which has recently attracted considerable interest is the sparsification approach [14]–[17]. This kind of method tries to find sparse representations of signal modes over a parameterized dictionary such as the Fourier or wavelet-based dictionary. It supposes that the signal modes can be well represented by the elements in the dictionary. However, if no priori information is available, it is rather difficult to determine the size of the dictionary which balances the tradeoff between the approximation accuracy and the computation load. We should mention that there are some other interesting methods sharing similar goal of this paper, such as the adaptive local iterative filtering method [18], the adaptive Fourier decomposition method [19], and the Blaschke decomposition method [20].

Since many real-world signals have compact Fourier spectrums, some methods propose to extract signal modes in the frequency domain. Methods of this class assume that the signal modes have narrow-band properties and have distinct spectrum support [21]. A representative method belonging to this class is the empirical wavelet transform (EWT). The EWT detects the spectrum support of each mode first and then recovers each mode by using wavelet filters corresponding to the supports [22]. The performance of the EWT depends heavily on the support detection algorithm. However, when the signal contains close modes, it is difficult to accurately identify the mode supports only through the spectrum information. More recently, Dragomiretskiy *et al.* proposed an adaptive data analysis method called variational mode decomposition (VMD) [23]. Unlike most methods that recursively recover each signal mode, the VMD simultaneously obtains all the modes through a joint-optimization scheme. As a result, the VMD has fine resolution to resolve close modes. The main issue of the VMD is that it is still formulated in the frequency domain, and thus it cannot

Manuscript received November 6, 2016; revised March 13, 2017 and April 29, 2017; accepted July 13, 2017. Date of publication July 24, 2017; date of current version September 19, 2017. The associate editor coordinating the review of this manuscript and approving it for publication was Dr. Pierre Borgnat. This work was supported in part by the National Natural Science Foundation of China under Grants 11632011 and 51121063, and in part by the Technology Innovation Program of Advanced Aerospace Technology Joint Center under Grant USCAST2016-26. *(Corresponding author: Zhike Peng.)*

The authors are with the State Key Laboratory of Mechanical System and Vibration, Shanghai Jiao Tong University, Shanghai 200240, China (e-mail: chenshiqian@sjtu.edu.cn; donxij@sjtu.edu.cn; z.peng@sjtu.edu.cn; wenmingz@sjtu.edu.cn; gmeng@sjtu.edu.cn).

Color versions of one or more of the figures in this paper are available online at http://ieeexplore.ieee.org.

Digital Object Identifier 10.1109/TSP.2017.2731300

decompose wide-band modes which have overlapping spectrums. Moreover, like EMD, the VMD can only separate modes, but cannot directly extract mode characteristics such as the instantaneous amplitude (IA) and the instantaneous frequency (IF).

Methods of the third class analyze NCSs using TF methods. Traditional TF analysis methods such as the short-time Fourier transform (STFT), the wavelet transform (WT), and the Wigner–Ville distribution often have poor TF resolution or suffer from cross-terms. Therefore, in the past decades, many efforts have been directed at improving the readability of time-frequency representations (TFRs) of NCSs. The reassignment technique is one of the most effective methods [24]. This method moves each value of a TFR from its original point to the center of gravity of the signal energy, to obtain a better localization of the signal. Recently, an improved version of this method, called the Levenberg-Marquardt reassignment, is proposed in [25] which makes the reassignment process adjustable. Although the reassignment improves the accuracy of the representation of signals, it cannot allow for the signal reconstruction. As a special case of reassignment, another well-known method called the synchrosqueezing transform (SST) can not only sharpen a TFR (i.e., improve its resolution) but also allow the retrieval of modes from the improved TFR [26]. However, the mode retrieval results by SST are derived based on strong assumptions that these modes are weakly modulated and well separated in the TF plane. Some work has been done to improve SST, such as the second-order SST designed to analyze signals with strong modulations [27], and the de-shape SST dealing with non-sinusoidal oscillatory signals [28]. Some other similar methods directly extract modes from ridge curves of linear TF transforms such as WT and STFT [29]–[31]. For these methods, the decomposition results are largely dependent on the resolution of the TFR and the ridge detection algorithm.

As discussed above, most existing methods are restricted to decomposing narrow-band modes which are well separated in the frequency or time-frequency domains. Inspired by VMD and the algorithmic framework of sparsification approach [15], [16], we introduce a method termed variational nonlinear chirp mode decomposition (VNCMD) to analyze wide-band NCSs composed of close or even crossed signal modes. The VNCMD is derived from the fact that a wide-band NCS can be transformed to a narrow-band signal through demodulation techniques. Therefore, we take advantage of this intrinsic feature of the NCS and formulate the decomposition problem as a demodulation problem. Namely, unlike the sparsification methods that rely on a parameterized model such as Fourier or wavelet based model [14], [16], [17], our method is fully non-parametric. Moreover, to analyze signals containing close modes, we adopt a similar joint-optimization scheme as the VMD to concurrently extract all the signal modes. Concretely, the VNCMD simultaneously searches for multiple modes which can optimally recover the observed signal, while these modes have the narrowest bands after being demodulated into baseband signals by the estimated IFs (of each mode). In fact, our method can be regarded as a TF filter bank with the center frequencies being the estimated IFs. Our optimization approach can be intuitively described as: for each mode, two demodulated quadrature signals can be iteratively updated by two filters with the current estimated IF; next, the IF can be further updated by the arctangent demodulation technique which provides the phase information of the two quadrature signals; the above two steps will be repeated until the demodulated signals have the narrowest bands.

The structure of the paper is organized as follows. In Section II, the signal model and some related notions are introduced. In Section III, we first detail the idea and the algorithm of the VNCMD, and then a simulated example is provided to demonstrate the algorithm. Section IV presents some experiment results to show advantages of our method. Our paper is concluded in Section V.

II. Background

A. Signal Model

The purpose of the VNCMD is to decompose a nonlinear chirp signal (NCS) into its constituent signal modes which we term as nonlinear chirp modes (NCMs). The definition of the NCM is provided as:

Definition 1: The NCMs are essentially AM-FM functions which can be expressed as

$$g(t) = a(t)\cos\left(2\pi\int_0^t f(s)\,ds + \phi\right) \tag{1}$$

where $a(t) > 0$, $f(t) > 0$ denote the instantaneous amplitude (IA) and the instantaneous frequency (IF) of the NCM, respectively; ϕ stand for the initial phase. The IA and IF of the NCM are assumed to be smooth functions which vary much slower than its phase function [26], [32], i.e., $|a'(t)|, |f'(t)| \ll |f(t)|$. It should be noted that a NCM may have a wide spectrum band since the IF can vary in a wide range. In other words, the NCM considered here may no longer obey the narrow-band property which has been extensively investigated in the literature [22], [23].

In practice, the collected signal consists of many NCMs and the measurement noise, and thus can be expressed as the following model:

$$g(t) = \sum_{i=1}^{Q} a_i(t)\cos\left(2\pi\int_0^t f_i(s)\,ds + \phi_i\right) + n(t) \tag{2}$$

where Q is the number of modes which is assumed to be known in this paper; $n \sim \mathcal{N}(0, \sigma^2)$ denotes the Gaussian white noise with the mean of zero and the variance of σ^2. It is important to note that the model (2) usually suffers from identifiability issues. That is, there may exist different representations for the given model (i.e., the IAs and IFs are not uniquely defined). It is an open problem. We can find a rigorous analysis of this problem in [33] which shows that the bias between two representations of the model will be small if the model satisfies some specific conditions (e.g., the slowly varying condition and positivity condition of the IA and IF in Definition 1).

B. Bandwidth of the NCM

In this subsection, we will introduce the bandwidth of the NCM which will be frequently discussed in this paper. It is known that the bandwidth of an AM-FM signal is closely related to its AM and FM behaviors. However, we do not find a rigorous definition of the bandwidth to describe such relationships. In this paper, we assume that the IA $a(t)$ is a band-limited function, and thus we can introduce an empirical definition as [23]:

Definition 2: The bandwidth of a NCM can be estimated as

$$BW = BW_{AM} + BW_{FM} \tag{3}$$

where $BW_{AM} = 2F_a$ denotes the bandwidth resulting from the AM, F_a stands for the maximum frequency of the IA $a(t)$; BW_{FM} is the bandwidth caused by the FM and it can be determined by the Carson's bandwidth rule [34]. Theoretically, any FM signal has an infinite number of sidebands, but more than 98% of the signal power is concentrated within the Carson's bandwidth in practice. Indeed, the IA $a(t)$ is also not always band-limited, but we assume that we can find a limited BW_{AM} which covers significant power of $a(t)$. Therefore, this definition is useful in practical applications, although it lacks a rigorous justification. Generally, the IA $a(t)$ is a slowly varying function. Therefore, for a wide-band NCM, its total bandwidth is often dominated by BW_{FM}, i.e.,

$$BW_{FM} \gg BW_{AM}. \tag{4}$$

C. Demodulation

Demodulation techniques can be used to remove the FM term of a NCM, thus resulting in a narrow-band demodulated signal [35]. First, the analytic signal of (1) is defined as

$$\begin{aligned} g_A(t) &= g(t) + j\mathbf{H}(g(t)) \\ &\approx a(t)\exp\left(j\left(2\pi\int_0^t f(s)\,ds + \phi\right)\right) \end{aligned} \tag{5}$$

where $j^2 = -1$; $\mathbf{H}(\cdot)$ denotes the Hilbert transform. Note that, for a practical NCM $g(t)$, the Hilbert transform does not provide its quadrature component. Therefore, in reality, we can only obtain the approximation result in (5) under some restrictive assumptions [36]. Then, we can define a pair of operators, called the demodulation operator (DO) and the modulation operator (MO), respectively, as [37]:

$$\Phi^-(t) = \exp\left(-j2\pi\left(\int_0^t f_d(s)\,ds - f_c t\right)\right) \tag{6}$$

$$\Phi^+(t) = \exp\left(j2\pi\left(\int_0^t f_d(s)\,ds - f_c t\right)\right) \tag{7}$$

where $f_d(s)$ denotes the frequency function of the operators, $f_c > 0$ is a constant frequency (we usually call it carrier frequency [35]). It is easy to find $\Phi^-(t)\cdot\Phi^+(t) = 1$. By multiplying $g_A(t)$ with the DO, we obtain a demodulated signal as

$$\begin{aligned} g_A^d(t) &= g_A(t)\,\Phi^-(t) \\ &= a(t)\exp\left(j\left(2\pi f_c t + 2\pi\int_0^t (f(s) - f_d(s))\,ds + \phi\right)\right). \end{aligned} \tag{8}$$

Note that $g_A^d(t)$ will become a purely AM signal centered around the carrier frequency f_c if we let $f_d(s) = f(s)$. In this case, the demodulated signal $g_A^d(t)$ will have the narrowest band as $BW_{\min} = BW_{AM}$ (see (3)) [38]–[40]. Fig. 1 provides spectrums of a NCM and its demodulated signal. It can be seen the demodulated signal has a more concentrated spectrum. The original analytic signal $g_A(t)$ can be recovered by multiplying $g_A^d(t)$ with the MO as

$$g_A(t) = g_A^d(t)\,\Phi^+(t). \tag{9}$$

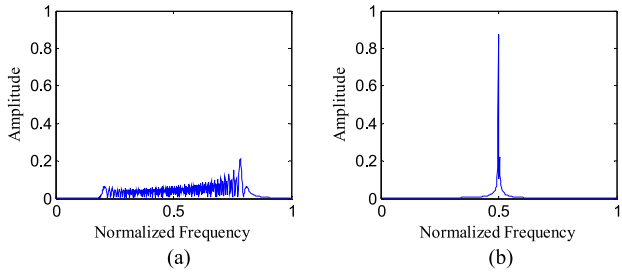

Fig. 1. Spectrums of a NCM and its demodulated signal. (a) NCM. (b) Demodulated signal.

In fact, the demodulation technique can also be applied to a real signal. By using the trigonometric identity, we can easily obtain the real forms of (8) and (9), respectively, as

$$\begin{aligned} \mathrm{Re}\left\{g_A^d(t)\right\} &= \mathrm{Re}\left\{g_A(t)\right\}\cdot\mathrm{Re}\left\{\Phi^-(t)\right\} \\ &\quad - \mathrm{Im}\left\{g_A(t)\right\}\cdot\mathrm{Im}\left\{\Phi^-(t)\right\} \end{aligned} \tag{10}$$

$$\begin{aligned} \mathrm{Re}\left\{g_A(t)\right\} &= \mathrm{Re}\left\{g_A^d(t)\right\}\cdot\mathrm{Re}\left\{\Phi^+(t)\right\} \\ &\quad - \mathrm{Im}\left\{g_A^d(t)\right\}\cdot\mathrm{Im}\left\{\Phi^+(t)\right\} \end{aligned} \tag{11}$$

where $\mathrm{Re}\{\cdot\}$ and $\mathrm{Im}\{\cdot\}$ stand for the real and imaginary parts, respectively.

III. VNCMD

In this section, we will first illustrate the main idea of our method and the detailed algorithm. Then, we will present a simulated example to demonstrate the method.

A. Main Idea

As mentioned before, we can transform a wide-band NCM into a narrow-band signal through the demodulation technique. Ideally, the demodulated signal will have the narrowest band if the frequency function of the DO is matched to that of the NCM (i.e., $f(s) = f_d(s)$ in (8)). Therefore, we can estimate the frequency information and also reconstruct a NCM

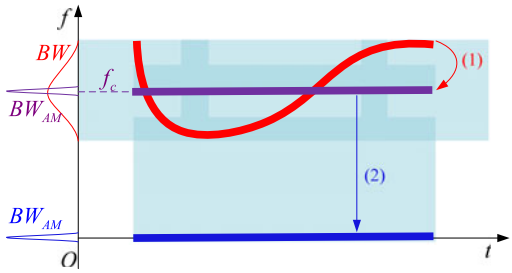

Fig. 2. Illustration of the demodulation scheme (the red, purple, and blue lines stand for the IF curves of the original, demodulated and baseband signals, respectively).

by minimizing the bandwidth of the demodulated signal. For a better understanding of the algorithm, we decompose our demodulation scheme into two steps, as illustrated in Fig. 2. In the first step, the FM term of a wide-band NCM is eliminated by the DO. That is, we can obtain the demodulated signal $g_A^d(t) = g_A(t)\exp(-j2\pi(\int_0^t f(s)ds - f_c t))$ which has the most compact spectrum (with the bandwidth of BW_{AM}) centered around the carrier frequency f_c. To evaluate the bandwidth of $g_A^d(t)$, we further demodulate $g_A^d(t)$ into the baseband signal $g_A^b(t) = g_A^d(t)\exp(-j2\pi f_c t)$ in the second step. Note that herein the DO (in the second step) $\exp(-j2\pi f_c t)$ acts as a frequency-shift operator which does not change the bandwidth of $g_A^d(t)$. The reason for obtaining the baseband signal is that its bandwidth can be easily evaluated by measuring its maximum frequency (or oscillation degree) [23]. It is worth noting that the two steps of the demodulation scheme can be put together into one step: $g_A^b(t) = g_A(t)\exp(-j2\pi\int_0^t f(s)ds)$ where $f(t)$ is the IF of the original NCM (see (1)). Therefore, our method is able to estimate the IF of a NCM by finding a smooth function $\tilde{f}(t)$ with which the obtained baseband signal has the narrowest band. It should be noted that the VMD method only involves the second step of the demodulation scheme above. As a result, the VMD can neither extract the IF of a NCM nor change its bandwidth.

To evaluate the bandwidth of a baseband signal, we follow the idea of some commonly used methods such as the Wiener filter [23] and the Vold-Kalman filter [41] to calculate the l_2 norm of the derivative of the signal. First, according to (11), the signal model in (2) can be rewritten into a new form as

$$g(t) = \sum_{i=1}^{Q} u_i(t)\cos\left(2\pi\int_0^t \tilde{f}_i(s)\,ds\right) + v_i(t)\sin\left(2\pi\int_0^t \tilde{f}_i(s)\,ds\right) + n(t) \quad (12)$$

where $u_i(t)$ and $v_i(t)$ are two demodulated signals given as

$$u_i(t) = a_i(t)\cos\left(2\pi\int_0^t \left(f_i(s) - \tilde{f}_i(s)\right)ds + \phi_i\right) \quad (13)$$

$$v_i(t) = -a_i(t)\sin\left(2\pi\int_0^t \left(f_i(s) - \tilde{f}_i(s)\right)ds + \phi_i\right) \quad (14)$$

where $\{\tilde{f}_i(t) : i = 1, \cdots, Q\}$ represent the frequency functions of DOs. Clearly, the IA can be recovered as $a_i(t) = \sqrt{{u_i}^2(t) + {v_i}^2(t)}$. Herein we employ the real signal model instead of the analytic model in (5) because, in practice, it only provides an approximation result and also the Hilbert transform of the signal data usually introduces end effects. Then, we can formulate our decomposition problem as

$$\min_{\{u_i(t)\},\{v_i(t)\},\{\tilde{f}_i(t)\}} \left\{\sum_{i=1}^{Q}\left(\|{u_i}''(t)\|_2^2 + \|{v_i}''(t)\|_2^2\right)\right\}$$
$$\text{s.t.} \left\| g(t) - \sum_{i=1}^{Q} u_i(t)\cos\left(2\pi\int_0^t \tilde{f}_i(s)\,ds\right) + v_i(t)\sin\left(2\pi\int_0^t \tilde{f}_i(s)\,ds\right)\right\|_2 \le \varepsilon \quad (15)$$

where we use the square of the l_2 norm of the second-order derivative to evaluate the signal bandwidth [41]; $\varepsilon > 0$ is an upper bound determined by the noise level. Note that, in practice, this formulation is only observed in discrete time. We will present the discrete formulation and the corresponding algorithm in next section. Formula (15) indicates that our method simultaneously searches for proper $\{\tilde{f}_i(t) : i = 1, \ldots, Q\}$ with which the demodulated signals $\{u_i(t) : i = 1, \ldots, Q\}$ and $\{v_i(t) : i = 1, \ldots, Q\}$ have the narrowest bands. As indicated in Definition 1, $\tilde{f}_i(t)$ is usually a smooth and slowly-varying function. However, it is difficult to explicitly include this condition in (15) because this formulation is highly nonlinear in $\tilde{f}_i(t)$. For simplicity, we try an expedient method to consider this condition by regulating the update of the IF (see (35) in the next subsection) during iterations [21]. Note that, if we let function $\tilde{f}_i(t)$ be a constant, the method will be equivalent to the VMD. Different from recursive mode extraction schemes [10]–[12], our method concurrently captures all the modes, which makes it have excellent resolution to separate close or even crossed signal modes.

B. Algorithm

In this subsection, we will present the detailed algorithm to solve the problem (15). Assuming that the data is sampled at $t = t_0, \ldots, t_{N-1}$, the discrete form of (15) can be obtained as

$$\min_{\{\boldsymbol{u}_i\},\{\boldsymbol{v}_i\},\{\boldsymbol{f}_i\}} \left\{\sum_i \left(\|\boldsymbol{\Omega}\boldsymbol{u}_i\|_2^2 + \|\boldsymbol{\Omega}\boldsymbol{v}_i\|_2^2\right)\right\}$$
$$\text{s.t.} \quad \left\|\boldsymbol{g} - \sum_i (\mathbf{A}_i\boldsymbol{u}_i + \mathbf{B}_i\boldsymbol{v}_i)\right\|_2 \le \varepsilon \quad (16)$$

where $\varepsilon = \sqrt{N\sigma^2}$; $\boldsymbol{u}_i = [u_i(t_0)\ldots u_i(t_{N-1})]^T$, $\boldsymbol{v}_i = [v_i(t_0)\ldots v_i(t_{N-1})]^T$, $\boldsymbol{f}_i = [\tilde{f}_i(t_0)\ldots\tilde{f}_i(t_{N-1})]^T$, $\boldsymbol{g} = [g(t_0)\ldots g(t_{N-1})]^T$;

$$\mathbf{A}_i = diag\left[\cos(\varphi_i(t_0))\ldots\cos(\varphi_i(t_{N-1}))\right] \quad (17)$$

$$\mathbf{B}_i = diag\left[\sin(\varphi_i(t_0))\ldots\sin(\varphi_i(t_{N-1}))\right] \quad (18)$$

where $\varphi_i(t) = 2\pi \int_0^t \tilde{f}_i(s)ds$; to alleviate the end effects caused by the difference operation, $\boldsymbol{\Omega}$ is a modified second-order difference operator given as

$$\boldsymbol{\Omega} = \begin{bmatrix} -1 & 1 & 0 & \cdots & 0 \\ 1 & -2 & 1 & \cdots & 0 \\ \vdots & \ddots & \ddots & \ddots & \vdots \\ 0 & \cdots & 1 & -2 & 1 \\ 0 & \cdots & 0 & 1 & -1 \end{bmatrix}. \tag{19}$$

In essence, the constraint set $\|\boldsymbol{g} - \sum_i (\mathbf{A}_i \boldsymbol{u}_i + \mathbf{B}_i \boldsymbol{v}_i)\|_2 \leq \varepsilon$ is an Euclidean ball with the center of zero and radius of ε:

$$\boldsymbol{\mathcal{C}}_\varepsilon \triangleq \left\{ \boldsymbol{c} \in \mathbb{R}^{N\times 1} : \|\boldsymbol{c}\|_2 \leq \varepsilon \right\}. \tag{20}$$

We further define the indicator function of the set (20) as

$$\mathcal{I}_{\boldsymbol{\mathcal{C}}_\varepsilon}(\boldsymbol{z}) \triangleq \begin{cases} 0, & \text{if } \boldsymbol{z} \in \boldsymbol{\mathcal{C}}_\varepsilon, \\ +\infty, & \text{if } \boldsymbol{z} \notin \boldsymbol{\mathcal{C}}_\varepsilon. \end{cases} \tag{21}$$

By introducing the auxiliary variable $\boldsymbol{w} \in \mathbb{R}^{N\times 1}$, we obtain an equivalent problem of (16) as

$$\begin{aligned} &\min_{\{\boldsymbol{u}_i\},\{\boldsymbol{v}_i\},\{\boldsymbol{f}_i\},\boldsymbol{w}} \left\{ \mathcal{I}_{\boldsymbol{\mathcal{C}}_\varepsilon}(\boldsymbol{w}) + \sum_i \left(\|\boldsymbol{\Omega}\boldsymbol{u}_i\|_2^2 + \|\boldsymbol{\Omega}\boldsymbol{v}_i\|_2^2 \right) \right\} \\ &\text{s.t.} \qquad \boldsymbol{w} = \boldsymbol{g} - \sum_i (\mathbf{A}_i \boldsymbol{u}_i + \mathbf{B}_i \boldsymbol{v}_i). \end{aligned} \tag{22}$$

Note that, as opposed to many methods such as the VMD, we explicitly take into account the influence of noise by including the noise variable $\boldsymbol{w}$ in the formula (22). As a result, our method will have better convergence and filtering (or de-noising) properties in noisy environments by comparison to alternative methods. To solve the constrained optimization problem (22), the corresponding augmented Lagrangian [15], [17], [23] is expressed as

$$\begin{aligned} L_\alpha(\{\boldsymbol{u}_i\},\{\boldsymbol{v}_i\},\{\boldsymbol{f}_i\},\boldsymbol{w},\lambda) &= \mathcal{I}_{\boldsymbol{\mathcal{C}}_\varepsilon}(\boldsymbol{w}) \\ &+ \sum_i \left(\|\boldsymbol{\Omega}\boldsymbol{u}_i\|_2^2 + \|\boldsymbol{\Omega}\boldsymbol{v}_i\|_2^2 \right) \\ &+ \lambda^T \left(\boldsymbol{w} + \sum_i (\mathbf{A}_i \boldsymbol{u}_i + \mathbf{B}_i \boldsymbol{v}_i) - \boldsymbol{g} \right) \\ &+ \frac{\alpha}{2} \left\| \boldsymbol{w} + \sum_i (\mathbf{A}_i \boldsymbol{u}_i + \mathbf{B}_i \boldsymbol{v}_i) - \boldsymbol{g} \right\|_2^2 \end{aligned} \tag{23}$$

which is equivalent to

$$\begin{aligned} L_\alpha(\{\boldsymbol{u}_i\},\{\boldsymbol{v}_i\},\{\boldsymbol{f}_i\},\boldsymbol{w},\lambda) &= \mathcal{I}_{\boldsymbol{\mathcal{C}}_\varepsilon}(\boldsymbol{w}) \\ &+ \sum_i \left(\|\boldsymbol{\Omega}\boldsymbol{u}_i\|_2^2 + \|\boldsymbol{\Omega}\boldsymbol{v}_i\|_2^2 \right) \\ &+ \frac{\alpha}{2} \left\| \boldsymbol{w} + \sum_i (\mathbf{A}_i \boldsymbol{u}_i + \mathbf{B}_i \boldsymbol{v}_i) - \boldsymbol{g} + \frac{1}{\alpha}\lambda \right\|_2^2 - \frac{1}{2\alpha}\|\lambda\|_2^2 \end{aligned} \tag{24}$$

where $\lambda \in \mathbb{R}^{N\times 1}$ is the Lagrangian multiplier, $\alpha > 0$ is a penalty parameter. Then, we can efficiently solve our problem using the well-known alternating direction method of multipliers (ADMM) [42]. The main idea of the ADMM is to decompose a complex optimization problem into several sub-problems in which each variable is updated separately. We will show how to solve these sub-problems in the following parts of this section. Note that, for notational simplicity, the iteration counters (i.e., superscripts like $\cdot^k$) for each variable are omitted. One should know that we always use the most recent updated variable in iterations.

The first step of our algorithm is to update the auxiliary variable (or called noise variable) $\boldsymbol{w}$. To do so, we need to solve the following sub-problem

$$\begin{aligned} \boldsymbol{w}^{k+1} &= \arg\min_{\boldsymbol{w}} \{L_\alpha(\{\boldsymbol{u}_i\},\{\boldsymbol{v}_i\},\{\boldsymbol{f}_i\},\boldsymbol{w},\lambda)\} \\ &= \arg\min_{\boldsymbol{w}} \left\{ \mathcal{I}_{\boldsymbol{\mathcal{C}}_\varepsilon}(\boldsymbol{w}) + \frac{\alpha}{2} \left\| \boldsymbol{w} + \sum_i (\mathbf{A}_i \boldsymbol{u}_i + \mathbf{B}_i \boldsymbol{v}_i) - \boldsymbol{g} + \frac{1}{\alpha}\lambda \right\|_2^2 \right\}. \end{aligned} \tag{25}$$

The solution of (25) can be obtained by the proximity operator which is defined as [43]:

$$\text{prox}_{\boldsymbol{\mathcal{C}}_\varepsilon/\alpha}(\boldsymbol{x}) \triangleq \arg\min_{\boldsymbol{w}} \left\{ \mathcal{I}_{\boldsymbol{\mathcal{C}}_\varepsilon}(\boldsymbol{w}) + \frac{\alpha}{2}\|\boldsymbol{w} - \boldsymbol{x}\|_2^2 \right\}. \tag{26}$$

Since $\mathcal{I}_{\boldsymbol{\mathcal{C}}_\varepsilon}(\boldsymbol{w})$ is the indicator function of the convex set $\boldsymbol{\mathcal{C}}_\varepsilon$, $\text{prox}_{\boldsymbol{\mathcal{C}}_\varepsilon/\alpha}(\boldsymbol{x})$ is equivalent to the projection onto $\boldsymbol{\mathcal{C}}_\varepsilon$, which is independent of the parameter α [44]. Namely, we have

$$\text{prox}_{\boldsymbol{\mathcal{C}}_\varepsilon/\alpha}(\boldsymbol{x}) = \mathcal{P}_{\boldsymbol{\mathcal{C}}_\varepsilon}(\boldsymbol{x}) \triangleq \begin{cases} \dfrac{\varepsilon}{\|\boldsymbol{x}\|_2} \cdot \boldsymbol{x}, & \text{if } \|\boldsymbol{x}\|_2 > \varepsilon, \\ \boldsymbol{x}, & \text{if } \|\boldsymbol{x}\|_2 \leq \varepsilon. \end{cases} \tag{27}$$

Therefore, the solution of (25) can be finally expressed as

$$\boldsymbol{w}^{k+1} = \mathcal{P}_{\boldsymbol{\mathcal{C}}_\varepsilon}\left(\boldsymbol{g} - \sum_i (\mathbf{A}_i \boldsymbol{u}_i + \mathbf{B}_i \boldsymbol{v}_i) - \frac{1}{\alpha}\lambda \right). \tag{28}$$

Next, we will update the two demodulated quadrature signals $\boldsymbol{u}_i$ and $\boldsymbol{v}_i$, respectively, as

$$\begin{aligned} \boldsymbol{u}_i^{k+1} &= \arg\min_{\boldsymbol{u}_i} \{L_\alpha(\{\boldsymbol{u}_m\},\{\boldsymbol{v}_m\},\{\boldsymbol{f}_m\},\boldsymbol{w},\lambda)\} \\ &= \arg\min_{\boldsymbol{u}_i} \left\{ \|\boldsymbol{\Omega}\boldsymbol{u}_i\|_2^2 + \frac{\alpha}{2} \left\| \boldsymbol{w} + \sum_m (\mathbf{A}_m \boldsymbol{u}_m + \mathbf{B}_m \boldsymbol{v}_m) - \boldsymbol{g} + \frac{1}{\alpha}\lambda \right\|_2^2 \right\} \end{aligned} \tag{29}$$

$$\begin{aligned} \boldsymbol{v}_i^{k+1} &= \arg\min_{\boldsymbol{v}_i} \{L_\alpha(\{\boldsymbol{u}_m\},\{\boldsymbol{v}_m\},\{\boldsymbol{f}_m\},\boldsymbol{w},\lambda)\} \\ &= \arg\min_{\boldsymbol{v}_i} \left\{ \|\boldsymbol{\Omega}\boldsymbol{v}_i\|_2^2 + \frac{\alpha}{2} \left\| \boldsymbol{w} + \sum_m (\mathbf{A}_m \boldsymbol{u}_m + \mathbf{B}_m \boldsymbol{v}_m) - \boldsymbol{g} + \frac{1}{\alpha}\lambda \right\|_2^2 \right\} \end{aligned} \tag{30}$$

We can easily find the solutions of (29) and (30) by setting their gradients to zero, yielding

$$\boldsymbol{u}_i^{k+1} = \underbrace{\left(\frac{2}{\alpha}\boldsymbol{\Omega}^T\boldsymbol{\Omega} + \mathbf{A}_i^T\mathbf{A}_i\right)^{-1}}_{\mathbf{H}_{c_i}}\mathbf{A}_i^T \cdot \underbrace{\left(\boldsymbol{g} - \sum_{m\neq i}\mathbf{A}_m\boldsymbol{u}_m - \sum_m \mathbf{B}_m\boldsymbol{v}_m - \boldsymbol{w} - \frac{1}{\alpha}\boldsymbol{\lambda}\right)}_{\boldsymbol{r}_{c_i}} \tag{31}$$

$$\boldsymbol{v}_i^{k+1} = \underbrace{\left(\frac{2}{\alpha}\boldsymbol{\Omega}^T\boldsymbol{\Omega} + \mathbf{B}_i^T\mathbf{B}_i\right)^{-1}}_{\mathbf{H}_{s_i}}\mathbf{B}_i^T \cdot \underbrace{\left(\boldsymbol{g} - \sum_{m}\mathbf{A}_m\boldsymbol{u}_m - \sum_{m\neq i} \mathbf{B}_m\boldsymbol{v}_m - \boldsymbol{w} - \frac{1}{\alpha}\boldsymbol{\lambda}\right)}_{\boldsymbol{r}_{s_i}} \tag{32}$$

where $\mathbf{H}_{c_i}, \mathbf{H}_{s_i}$ act as two low-pass filters; $\boldsymbol{r}_{c_i}, \boldsymbol{r}_{s_i}$ denote two residual signals which only contain concerned signals (i.e., all other signals and noise have been subtracted). Using the results in (31) and (32), we can update the corresponding mode as

$$\boldsymbol{g}_i^{k+1} = \mathbf{A}_i\boldsymbol{u}_i^{k+1} + \mathbf{B}_i\boldsymbol{v}_i^{k+1} = \mathbf{A}_i\mathbf{H}_{c_i}\mathbf{A}_i^T\boldsymbol{r}_{c_i} + \mathbf{B}_i\mathbf{H}_{s_i}\mathbf{B}_i^T\boldsymbol{r}_{s_i}. \tag{33}$$

Remark: Since we use the same index (i.e., the l_2 norm of the second-order derivative) as the Vold-Kalman filter (VKF) to assess the bandwidth, our method can be viewed as a time-frequency (TF) filter bank in which each filter shares similar properties with the VKF [41]. Equation (33) shows that each mode is updated by applying two TF filters (i.e., $\mathbf{A}_i\mathbf{H}_{c_i}\mathbf{A}_i^T$ and $\mathbf{B}_i\mathbf{H}_{s_i}\mathbf{B}_i^T$) to the residual signals (i.e., $\boldsymbol{r}_{c_i}$, and $\boldsymbol{r}_{s_i}$). The TF filters are obtained by modulating the low-pass filters (i.e., $\mathbf{H}_{c_i}$ and $\mathbf{H}_{s_i}$) with the current estimated IF (included in $\mathbf{A}_i$ and $\mathbf{B}_i$). Clearly, the center frequency of the TF filters is the estimated IF, and the bandwidth is determined by the penalty parameter α. Choosing a smaller α means that the obtained signal is smoother, i.e., the filter has a narrower pass band.

Next, we will address the issue of updating the IF by using the results in (31) and (32). It is clear that the IF of the two demodulated signals provides the increment for the IF update (see (13) and (14)). Therefore, we can obtain the IF increment through the arctangent demodulation technique as [16], [17], [45], [46]:

$$\begin{aligned}\Delta\tilde{f}_i^{k+1}(t) &= -\frac{1}{2\pi}\frac{d}{dt}\left(\arctan\left(\frac{v_i^{k+1}(t)}{u_i^{k+1}(t)}\right)\right)\\ &= \frac{v_i^{k+1}(t)\cdot\left(u_i^{k+1}(t)\right)' - u_i^{k+1}(t)\cdot\left(v_i^{k+1}(t)\right)'}{2\pi\left(\left(u_i^{k+1}(t)\right)^2 + \left(v_i^{k+1}(t)\right)^2\right)}.\end{aligned} \tag{34}$$

Since the IF is typically a smooth function [21], we assume that the IF increment in each iteration is still a band-limited function which admits

$$\min_{\Delta\boldsymbol{f}_i^{k+1}}\left\{\left\|\boldsymbol{\Omega}\Delta\boldsymbol{f}_i^{k+1}\right\|_2^2 + \frac{\mu}{2}\left\|\Delta\boldsymbol{f}_i^{k+1} - \Delta\tilde{\boldsymbol{f}}_i^{k+1}\right\|_2^2\right\} \tag{35}$$

where $\Delta\tilde{\boldsymbol{f}}_i^{k+1} = [\Delta\tilde{f}_i^{k+1}(t_0), \ldots, \Delta\tilde{f}_i^{k+1}(t_{N-1})]^T$ denotes the calculated increment by (34), $\Delta\boldsymbol{f}_i^{k+1}$ is the desired one, μ is a penalty parameter. The solution of (35) is

$$\Delta\boldsymbol{f}_i^{k+1} = \left(\frac{2}{\mu}\boldsymbol{\Omega}^T\boldsymbol{\Omega} + \mathbf{I}\right)^{-1}\Delta\tilde{\boldsymbol{f}}_i^{k+1} \tag{36}$$

where $\mathbf{I}$ denotes an identity matrix. Based on the results above, we can finally update the IF as

$$\boldsymbol{f}_i^{k+1} = \boldsymbol{f}_i^k + \gamma\cdot\Delta\boldsymbol{f}_i^{k+1} \tag{37}$$

where $0 < \gamma < 1$ is a proportionality factor employed to stabilize the algorithm. In our simulations, we let $\gamma = 0.5$ which provides good results.

The last step of our algorithm is to update the Lagrangian multiplier as

$$\boldsymbol{\lambda}^{k+1} = \boldsymbol{\lambda}^k + \alpha\left(\boldsymbol{w}^{k+1} + \sum_i \boldsymbol{g}_i^{k+1} - \boldsymbol{g}\right). \tag{38}$$

In our experiments, we find that the iterative algorithm presented above may easily diverge if the initial IFs are chosen too far from the true IFs. It is known that restart techniques have been widely employed to accelerate and stabilize a numerical algorithm [47]. Therefore, we propose to incorporate a restart scheme into our algorithm. That is, if the residual energy $\|\boldsymbol{w}^{k+1} + \sum_i \boldsymbol{g}_i^{k+1} - \boldsymbol{g}\|_2^2$ is larger than a threshold (i.e., the signal energy $\|\boldsymbol{g}\|_2^2$ in this paper), we will reset the Lagrangian multiplier and the demodulated signals while the estimated IFs will remain unchanged. This restart scheme will ensure the algorithm have good convergence performance. Our complete decomposition algorithm is outlined in Algorithm 1. Herein we want to mention that the computation load of the algorithm mainly comes from the matrix operations (i.e., matrix multiplication and inversion; e.g., see (31), (32) and (36)). Fortunately, most elements of these matrices (i.e., $\boldsymbol{\Omega}$, $\mathbf{A}_i$, $\mathbf{B}_i$ in (16)) are zeros. Therefore, we can use the sparse forms of these matrices (generated by the MATLAB function *spdiags*; namely, only the non-zero elements are stored) which can significantly reduce the computational cost of the method.

It should be noted that our optimization scheme introduced above is not a standard ADMM because the matrices $\mathbf{A}_i, \mathbf{B}_i$ depend nonlinearly on the variables $\boldsymbol{u}_i, \boldsymbol{v}_i$ in (16). The theoretical analysis of the convergence is not possible in the present paper. We will test the convergence performance of our method in Section III-C through simulation experiments. Herein we want to make some comments on choice of the two penalty parameters (i.e., α and μ) of the algorithm. In practice, we suggest increasing the bandwidth of the TF filters by choosing a larger α, if the signal modes are well separated. This will help the algorithm to capture the correct modes even when the initial IFs are too rough (i.e., far from the true IFs). However, increasing

Algorithm 1: VNCMD.

Initialize $\boldsymbol{g}$; α; μ; $\boldsymbol{f}_i^1$, $\mathbf{A}_i^1 \leftarrow diag[\cos(2\pi \int f_i^1(t)dt)]$, $\mathbf{B}_i^1 \leftarrow diag[\sin(2\pi \int f_i^1(t)dt)]$, $\boldsymbol{u}_i^1 \leftarrow (\frac{2}{\alpha}\boldsymbol{\Omega}^T\boldsymbol{\Omega} + (\mathbf{A}_i^1)^T\mathbf{A}_i^1)^{-1}(\mathbf{A}_i^1)^T\boldsymbol{g}$, $\boldsymbol{v}_i^1 \leftarrow (\frac{2}{\alpha}\boldsymbol{\Omega}^T\boldsymbol{\Omega} + (\mathbf{B}_i^1)^T\mathbf{B}_i^1)^{-1}(\mathbf{B}_i^1)^T\boldsymbol{g}$, for $i = 1, \cdots, Q$; $\boldsymbol{\lambda}^1 \leftarrow \mathbf{0}$; $k \leftarrow 0$.
repeat
  $k \leftarrow k + 1$
  $\boldsymbol{w}^{k+1} \leftarrow \mathcal{P}_{\mathcal{C}_\varepsilon}(\boldsymbol{g} - \sum_i (\mathbf{A}_i^k\boldsymbol{u}_i^k + \mathbf{B}_i^k\boldsymbol{v}_i^k) - \frac{1}{\alpha}\boldsymbol{\lambda}^k)$
  for $i \leftarrow 1$ **to** Q
    $\boldsymbol{u}_i^{k+1} \leftarrow \arg\min_{\boldsymbol{u}_i}\{L_\alpha(\{\boldsymbol{u}_{m<i}^{k+1}, \boldsymbol{u}_{m\geq i}^k\}, \{\boldsymbol{v}_{m<i}^{k+1}, \boldsymbol{v}_{m\geq i}^k\}, \{\boldsymbol{f}_{m<i}^{k+1}, \boldsymbol{f}_{m\geq i}^k\}, \boldsymbol{w}^{k+1}, \boldsymbol{\lambda}^k)\}$
    $\boldsymbol{v}_i^{k+1} \leftarrow \arg\min_{\boldsymbol{v}_i}\{L_\alpha(\{\boldsymbol{u}_{m\leq i}^{k+1}, \boldsymbol{u}_{m>i}^k\}, \{\boldsymbol{v}_{m<i}^{k+1}, \boldsymbol{v}_{m\geq i}^k\}, \{\boldsymbol{f}_{m<i}^{k+1}, \boldsymbol{f}_{m\geq i}^k\}, \boldsymbol{w}^{k+1}, \boldsymbol{\lambda}^k)\}$
    $\Delta\tilde{f}_i^{k+1}(t) \leftarrow \frac{v_i^{k+1}(t)\cdot(u_i^{k+1}(t))' - u_i^{k+1}(t)\cdot(v_i^{k+1}(t))'}{2\pi((u_i^{k+1}(t))^2 + (v_i^{k+1}(t))^2)}$
    $\boldsymbol{f}_i^{k+1} \leftarrow \boldsymbol{f}_i^k + \frac{1}{2}(\frac{2}{\mu}\boldsymbol{\Omega}^T\boldsymbol{\Omega} + \mathbf{I})^{-1}\Delta\tilde{\boldsymbol{f}}_i^{k+1}$
    $\mathbf{A}_i^{k+1} \leftarrow diag[\cos(2\pi \int f_i^{k+1}(t)dt)]$
    $\mathbf{B}_i^{k+1} \leftarrow diag[\sin(2\pi \int f_i^{k+1}(t)dt)]$
    $\boldsymbol{g}_i^{k+1} \leftarrow \mathbf{A}_i^{k+1}\boldsymbol{u}_i^{k+1} + \mathbf{B}_i^{k+1}\boldsymbol{v}_i^{k+1}$
  end for
  $\boldsymbol{\lambda}^{k+1} \leftarrow \boldsymbol{\lambda}^k + \alpha(\boldsymbol{w}^{k+1} + \sum_i \boldsymbol{g}_i^{k+1} - \boldsymbol{g})$
  if $\|\boldsymbol{w}^{k+1} + \sum_i \boldsymbol{g}_i^{k+1} - \boldsymbol{g}\|_2^2 > \|\boldsymbol{g}\|_2^2$ **then**
    $\boldsymbol{\lambda}^{k+1} \leftarrow \mathbf{0}$
    for $i \leftarrow 1$ **to** Q
      $\boldsymbol{u}_i^{k+1} \leftarrow (\frac{2}{\alpha}\boldsymbol{\Omega}^T\boldsymbol{\Omega} + (\mathbf{A}_i^{k+1})^T\mathbf{A}_i^{k+1})^{-1}(\mathbf{A}_i^{k+1})^T\boldsymbol{g}$
      $\boldsymbol{v}_i^{k+1} \leftarrow (\frac{2}{\alpha}\boldsymbol{\Omega}^T\boldsymbol{\Omega} + (\mathbf{B}_i^{k+1})^T\mathbf{B}_i^{k+1})^{-1}(\mathbf{B}_i^{k+1})^T\boldsymbol{g}$
    end for
  end if
until $\sum_i \|\boldsymbol{g}_i^{k+1} - \boldsymbol{g}_i^k\|_2^2 / \|\boldsymbol{g}_i^k\|_2^2 \leq \delta$

the bandwidth also indicates that the obtained modes will contain more noise [23]. In the case that the signal is composed of closely spaced modes, one should choose a smaller α to alleviate the interference between adjacent modes. As for the penalty parameter μ, choosing a smaller μ (i.e., ensuring a smoother IF increment in (36)) will benefit the convergence process of the algorithm, while, in some cases, one may require a larger μ to capture fast varying IFs. In practice, a more effective scheme is to gradually increase μ from a relatively small value to a desired larger value during the iterations [16].

C. Demonstration

To show the validity of the algorithm, herein we consider a NCS consisting of one mode and the Gaussian white noise $n(t)$ as

$$g_n(t) = \cos\left(2\pi\left(1.5 + 150t - 100t^2 + 416t^3 - 200t^4\right)\right) + n(t) \tag{39}$$

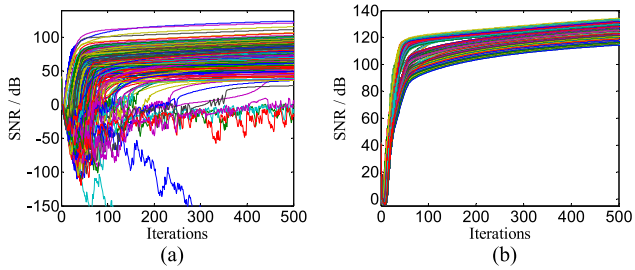

Fig. 3. Convergence curves with 500 random initial IFs in the noise-free case (i.e., $\sigma = 0$). (a) Traditional ADMM. (b) Improved ADMM with the restart scheme.

where the IF of the mode is $f(t) = 150 - 200t + 1248t^2 - 800t^3$, the variance of $n(t)$ is denoted by σ^2. The sampling frequency is 2000 Hz and the time duration is 1 s. We define the relative error (RE) for IF estimation as

$$\mathrm{RE} = \frac{\left\|\tilde{f}(t) - f(t)\right\|_2}{\|f(t)\|_2} \tag{40}$$

where $\tilde{f}(t)$ is the estimated IF, $f(t)$ stands for the true one. Analogously, we can define the signal-to-noise ratio (SNR) to measure the accuracy of mode reconstruction as

$$\mathrm{SNR} = 20\log_{10}\left(\frac{\|g(t)\|_2}{\|\tilde{g}(t) - g(t)\|_2}\right) \tag{41}$$

where the unit of the SNR is dB.

First, we want to test the convergence performance of the algorithm through the example (39). In fact, the algorithm will not always converge to the correct results when the signal is contaminated by strong noise and when rough initial IFs are specified. That is, the convergence properties rely on the specified IFs and also the noise level. In the first test, we generate 500 random initial IFs of the form $f_{ini}(t) = f(t) + e_r$ where $f(t)$ denotes the true IF; $e_r \in [1, 500]$ is a random error (i.e., according to (40), the maximum RE of the initial IFs is 176.8%). Then, we test the convergence results of the algorithm with these random IFs in the noise-free case (i.e., let $\sigma = 0$). Herein we set α and μ to 1e-2 and 1e-10, respectively. Fig. 3 provides the convergence curves (with respect to the SNRs of the estimated modes) by the tradition ADMM and our algorithm with the restart scheme. It shows that the traditional ADMM has a much slower convergence speed and may likely diverge with rough initializations. Conversely, our algorithm can converge to good results (e.g., when SNR $>$ 60 dB) quickly even with roughly specified IFs.

Then, we will test the performance of the algorithm under different noise levels. We set the maximum allowable iterations and the convergence tolerance δ to 500 and 1e-8, respectively. In this case, the initial IFs have deterministic offset errors as 100, 150, 170, 200, and 250 Hz, respectively (i.e., the corresponding REs are 35.4%, 53.0%, 60.1%, 70.7%, and 88.4% (see (40))). With these initializations, we execute our algorithm for 100 times at each noise level and obtain the success rate as shown in Fig. 4(a). Herein we think one execution is successful only when the RE of the final estimated IF is less than 1%. Fig. 4(a) shows that the algorithm still has a high success rate at a strong noise

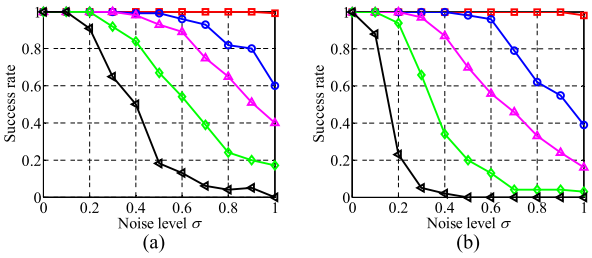

Fig. 4. Success rate at different noise levels (the red, blue, purple, green, and black lines denote the results when the REs of the initial IFs are 35.4%, 53.0%, 60.1%, 70.7%, and 88.4%, respectively). (a) Complete algorithm. (b) Algorithm with $\boldsymbol{w} = \mathbf{0}$ and $\boldsymbol{\lambda} = \mathbf{0}$ (i.e., dropping the noise variable and the Lagrangian multiplier).

level (e.g., $\sigma = 0.6$) when the RE of the initial IF is less than 60%. This condition can be easily satisfied if prior information on the signal is available. In practice, if the signal is too noisy, one can still provide a relatively good initial IF by detecting spectrum peaks [22] or TF ridges [21], [29].

It should be noted that, in practical applications, we need to estimate the noise level σ in advance. A correct σ ensures the algorithm have good convergence and filtering (or de-noising) properties in noisy environments. If the estimated σ is smaller than the ground truth, more noise will be included in the reconstructed modes. On the other hand, specifying a much larger σ (than the true one) will result in serious energy loss of the modes and may cause the stability issue. For simplicity, one can get a coarse estimate of σ by using wavelet decomposition. Herein we suggest a more accurate method in [48] which estimates the noise variance in the TF domain. Indeed, we want to mention that it is not always possible to find a desired σ to clearly describe the noise property (e.g., when the noise is nonwhite and non-Gaussian). In this case, enforcing the strict constraint in (16) is not a good choice. Therefore, an expedient method is to drop the noise variable $\boldsymbol{w}$ and the Lagrangian multiplier λ (i.e., let $\boldsymbol{w} = \mathbf{0}$ and $\boldsymbol{\lambda} = \mathbf{0}$ in (23)) to get a least-squares approximation [23]. This strategy can also provide acceptable de-noising properties and can make the proposed method adapt to more complicated situations. Note that if we drop $\boldsymbol{w}$ only (i.e., $\boldsymbol{w} = \mathbf{0}$ and $\boldsymbol{\lambda} \neq \mathbf{0}$), we will essentially enforce an equality constraint $\boldsymbol{g} = \sum_i (\mathbf{A}_i \boldsymbol{u}_i + \mathbf{B}_i \boldsymbol{v}_i)$ in (16). That is, more unwanted components (e.g., noise) will be included. We provide the success rate of the algorithm with $\boldsymbol{w} = \mathbf{0}$ and $\boldsymbol{\lambda} = \mathbf{0}$ in Fig. 4(b). Indeed, the simplified algorithm performs much worse than the original algorithm (see Fig. 4(a) and (b)) especially when rough initial IFs are specified. But if good initializations are provided, it can still have a high success rate.

Next, the VNCMD is compared with the VMD and a recently introduced method (called De-VSST) [37] for mode reconstruction. The De-VSST combines a demodulation technique with the vertical second-order SST (VSST) [27], which shows good results to reconstruct modes with strong modulations. Herein we let $\sigma = 0.5$ and the SNR of the noisy signal is 3.01 dB. The initial IF of the VNCMD is roughly set to 200 Hz. The estimated modes and IFs by different methods are illustrated in Fig. 5. As discussed before, the VMD is in essence a filter bank working in the frequency domain. To recover a wide-band signal, one

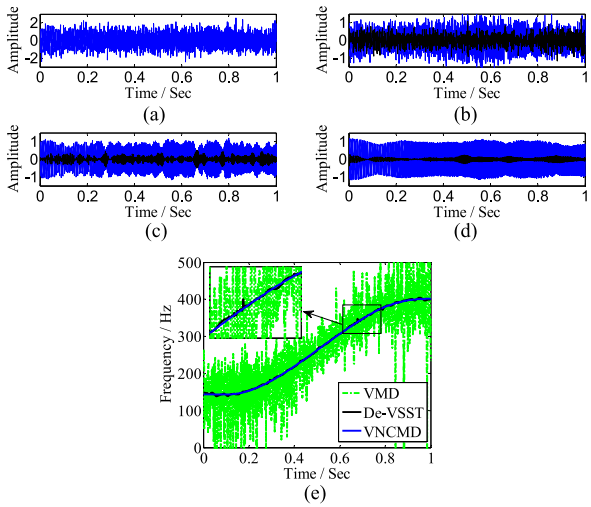

Fig. 5. Noisy signal in (39) and the analysis results. (a) Noisy signal (SNR: 3.01 dB). (b)–(d) give the estimated signals by the VMD, De-VSST and VNCMD, respectively (blue: estimated signals; black: estimation errors; the SNRs of these signals are 7.25, 13.47, and 18.48 dB, respectively). (e) Estimated IFs (the REs of the IFs by VMD, De-VSST, and VNCMD are 21.75%, 0.55%, and 0.32%, respectively).

should increase the bandwidth of the VMD, which inevitably introduces more noise, as shown in Fig. 5(b). The reconstructed mode by De-VSST is a little bit noisy and the reconstruction result for this example should still be improved (see Fig. 5(c)). For the VNCMD, the noise level σ is estimated as 0.4967 by the method in [48] and the reconstructed mode with the estimated σ is provided in Fig. 5(d). As a TF filter bank, the VNCMD only retains the information near the IF curve and effectively excludes most of the noise. In addition, the projection operation in (28) also helps to suppress the noise. Therefore, the SNR of the estimated signal can be significantly improved (see Fig. 5(d)). Fig. 5(e) provides the IF estimation results by different methods. For VMD, we extract the IF from the estimated signal by the Hilbert transform (because the VMD cannot directly estimate the IF). It can be seen the Hilbert transform is sensitive to noise and one cannot get valuable information from the result. The De-VSST estimates IFs by detecting ridge curves of the VSST (herein we use the ridge detector in [49]). One can observe that the estimated IF curve shows slight oscillations due to the noise perturbation. On the contrary, the VNCMD can obtain a rather smoother IF. This test shows that the proposed method has good performance in a noisy environment.

IV. Examples and Discussions

In this section, we will apply the VNCMD to analyze some more complicated signals including three artificial signals and two real signals from whale sounds.

A. *Artificial Signals*

Three examples containing close or even crossed modes will be considered in this subsection. Since different modes are closely spaced in these cases, we suggest choosing a small α (e.g., 1e-6 $\leq \alpha \leq$ 1e-5 according to our experiments) as

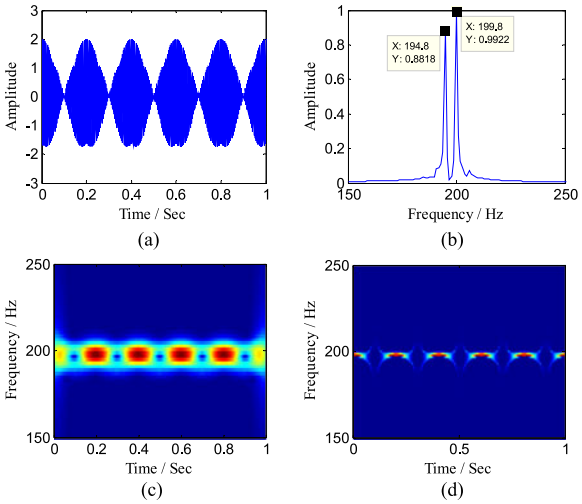

Fig. 6. Signal in (42). (a) Waveform. (b) Fourier spectrum. (c) TFR by STFT. (d) TFR by VSST.

discussed in Section III-C; μ is gradually increased from a very small value (e.g., 1e-10) to a larger value (e.g., α) in iterations; the convergence tolerance δ is set to 1e-8.

The first simulated signal is composed of two narrow-band modes (see Fig. 6):

$$g_{sig1}(t) = g_{m1}(t) + g_{m2}(t) \tag{42}$$

with

$$g_{m1}(t) = \cos\left(390\pi t + 0.2\sin\left(10\pi t\right)\right) \tag{43}$$

$$g_{m2}(t) = \cos\left(400\pi t + 0.2\sin\left(10\pi t\right)\right) \tag{44}$$

where the IFs, i.e., $f_{m1}(t) = 195 + \cos(10\pi t)$ and $f_{m2}(t) = 200 + \cos(10\pi t)$ exhibit very slight oscillations. The number of the samples is 1000. It can be seen the two modes are so close to each other that the sum of the modes shows AM phenomenon (introduced by the beat effect) (see Fig. 6(a)). Fig. 6(c) and (d) display TFRs obtained by the short-time Fourier transform (STFT) and VSST, respectively. These methods cannot tell the two modes apart due to the poor resolution. Then, we apply our method and the VMD to decompose the signal. In this case, the initial IFs are specified by detecting the spectrum peaks (see Fig. 6(b)), i.e., 194.8 Hz for m1 and 199.8 Hz for m2. The results are shown in Fig. 7. In fact, there exists interference between the spectrums of the close modes due to the leakage. Therefore, the VMD cannot fully separate the two modes because it is directly formulated in the frequency domain (e.g., the estimated m2 includes unwanted portions from the m1 as shown in Fig. 7(a)). Our method solves the optimization problems in the time domain and can accurately recover the two modes (see Fig. 7(b)). Fig. 7(c) and (d) provide the estimated IFs by the VMD and VNCMD, respectively. The VMD extracts the IFs through the Hilbert transform which introduces serious boundary effects. The VNCMD accurately estimates such weak oscillations of the IF curves, which shows great potential in industrial applications, such as micro-Doppler signature extractions. In this example, the VNCMD requires 166 iterations and it totally takes about 0.6 s; the VMD requires about 1.6 s.

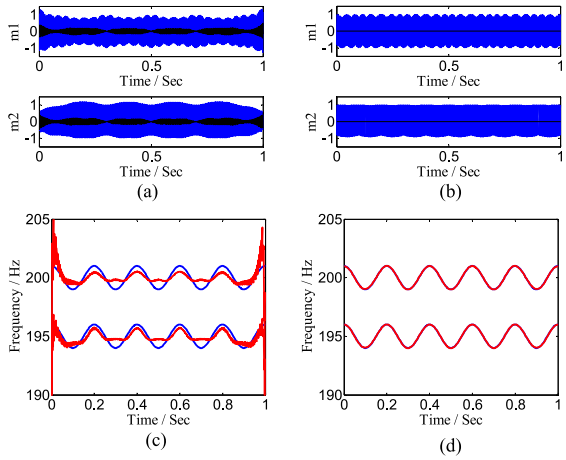

Fig. 7. Analysis results for the signal in (42). (a) and (b) show the estimated modes by the VMD and VNCMD, respectively (blue: estimated modes; black: estimation errors). (c) and (d) display the estimated IFs by the VMD and VNCMD, respectively (blue: true; red: estimated).

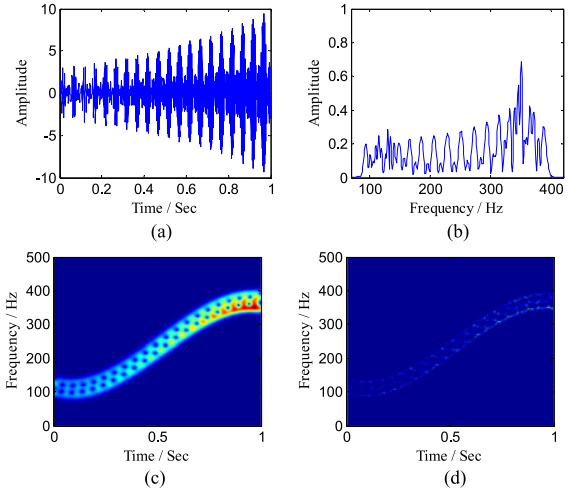

Fig. 8. Signal in (45). (a) Waveform. (b) Fourier spectrum. (c) TFR by STFT. (d) TFR by VSST.

The second example contains three wide-band modes whose IFs have a similar form to that of (39) (see Fig. 8):

$$g_{sig2}(t) = g_{m1}(t) + g_{m2}(t) + g_{m3}(t) \tag{45}$$

with

$$g_{m1}(t) = \exp(0.8t) \times \cos\left(2\pi\left(0.8 + 140t - 100t^2 + 416t^3 - 200t^4\right)\right) \tag{46}$$

$$g_{m2}(t) = \exp(1.2t) \times \cos\left(2\pi\left(1.2 + 120t - 100t^2 + 416t^3 - 200t^4\right)\right) \tag{47}$$

$$g_{m3}(t) = \exp(1.5t) \times \cos\left(2\pi\left(1.5 + 100t - 100t^2 + 416t^3 - 200t^4\right)\right) \tag{48}$$

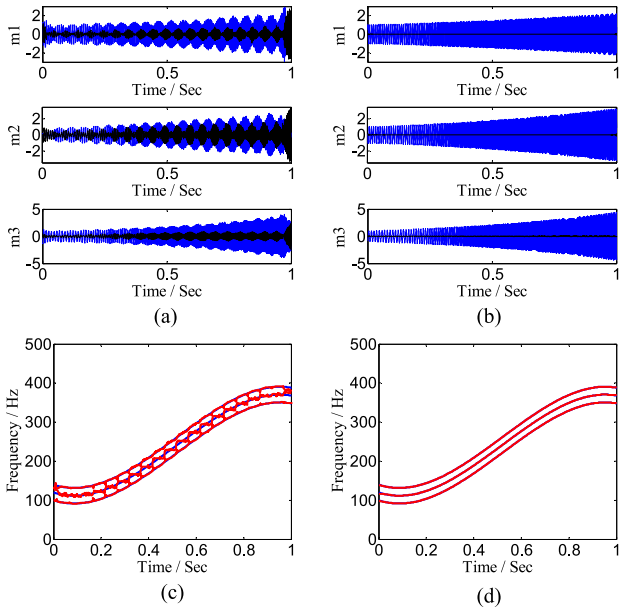

Fig. 9. Analysis results for the signal in (45). (a) and (b) show the estimated modes by the De-VSST and VNCMD, respectively (blue: estimated modes; black: estimation errors). (c) and (d) show the estimated IFs by the De-VSST and VNCMD, respectively (blue: true; red: estimated).

where these modes are overlapping in the frequency domain and thus the VMD cannot analyze this example. The number of the samples is 2000. As shown in Fig. 8(c) and (d), there exists serious reticulate interference between the modes in the TFRs because these signal modes are very close to each other. The decomposition results by the De-VSST and VNCMD are provided in Fig. 9 where (for the VNCMD) the initial IFs of these modes are roughly set to 500, 100, and 20 Hz, respectively. The De-VSST introduces serious boundary effects, and it shows large reconstruction errors (especially for m2) due to interference of different modes. The VNCMD shows high accuracy for reconstructing these close modes and extracting their IFs as shown in Fig. 9(b) and (d). In this example, the VNCMD requires 91 iterations and it takes about 0.85 s; the De-VSST takes about 6 s to extract one mode.

The third signal is composed of two modes whose IFs cross in the TF plane (see Fig. 10):

$$g_{sig3}(t) = g_{m1}(t) + g_{m2}(t) \tag{49}$$

with

$$g_{m1}(t) = a(t)\cos\left(2\pi\left(0.2 + 532t - 474t^2 + 369t^3\right)\right) \tag{50}$$

$$g_{m2}(t) = a(t)\cos\left(2\pi\left(0.8 + 50t + 525t^2 - 300t^3\right)\right) \tag{51}$$

where $a(t) = 1 + 0.5\cos(2\pi t)$ denotes the IA of the modes. The number of the samples is 2000. Obviously, these wideband modes are still overlapping in the frequency domain, and the VMD is not considered in this example either. It can be seen both the STFT and the VSST cannot clearly reveal the TF pattern of the signal in the crossing region (i.e., during 0.4∼0.6 s) as shown in Fig. 10(c) and (d).

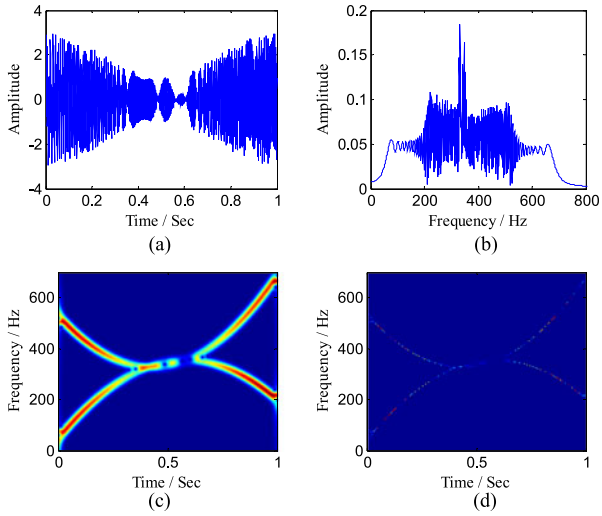

Fig. 10. Signal in (49). (a) Waveform. (b) Fourier spectrum. (c) TFR by STFT. (d) TFR by VSST.

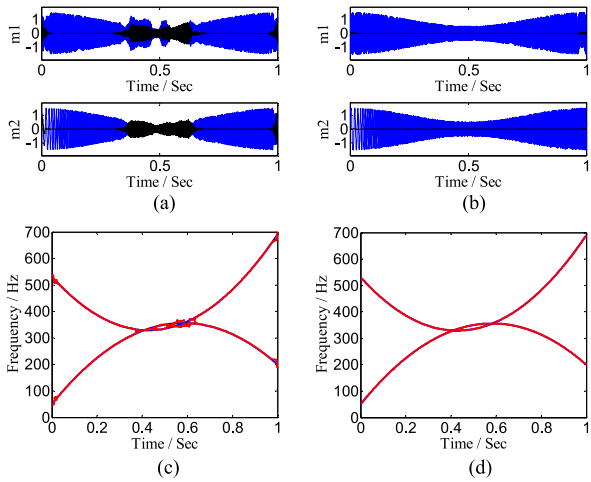

Fig. 11. Analysis results for the signal in (49). (a) and (b) show the estimated modes by the De-VSST and VNCMD, respectively (blue: estimated modes; black: estimation errors). (c) and (d) illustrate the estimated IFs by the De-VSST and VNCMD, respectively (blue: true; red: estimated).

For our method, the initial IFs are set to be 700 and 20 Hz. The analysis results are shown in Fig. 11. We can observe that the De-VSST fails to retrieve the modes and capture their IFs near the intersection portions. Conversely, our method successfully separates the crossed modes and accurately identifies the IFs (see Fig. 11(b) and (d)). For the crossed modes, the VNCMD requires more iterations (i.e., 282) and it takes about 1.5 s; the De-VSST takes about 6 s to extract one mode.

The SNRs (see (41)) of the reconstructed modes and the REs (see (40)) of the estimated IFs for the three examples above are listed in Tables I and II, respectively. These examples show potential of our method in decomposing the signals with close and crossed modes.

B. Real-Life Signals

In this subsection, we will apply the proposed method to decompose two real signals from the whistles of killer whales

TABLE I
SNRs OF THE ESTIMATED MODES

		VMD	De-VSST	VNCMD
(42)	m1	15.26	-	48.27
	m2	15.11	-	48.24
(45)	m1	-	9.06	42.20
	m2	-	7.01	39.33
	m3	-	12.79	43.15
(49)	m1	-	11.13	43.83
	m2	-	11.19	45.32

TABLE II
RES OF THE ESTIMATED IFS

		VMD	De-VSST	VNCMD
(42)	m1	7.77e-3	-	8.30e-5
	m2	1.78e-2	-	8.41e-5
(45)	m1	-	8.81e-3	5.30e-4
	m2	-	1.84e-2	1.40e-3
	m3	-	6.51e-3	6.57e-4
(49)	m1	-	8.47e-3	6.96e-4
	m2	-	1.18e-2	8.54e-4

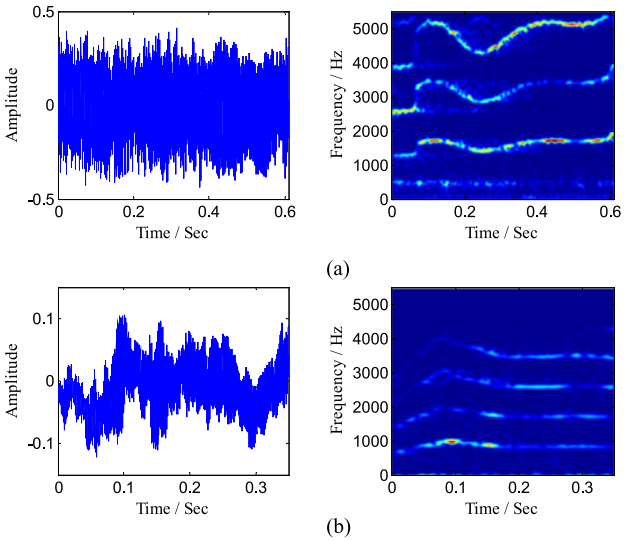

Fig. 12. Whale whistles. (a) S1. (b) S2.

[50]. The whales use sound for echolocation and communication. Therefore, analyzing these sound signals becomes very important in studying the behaviors of the whales. The two whistle signals are provided in Fig. 12 where the signals are denoted by S1 and S2, respectively. Both signals are contaminated by background noise. We can observe that S1 has more complex IFs while S2 contains a complicated trend mode. The analysis results by the proposed method are shown in Fig. 13 in which the estimated modes of each signal are arranged from low frequency to high frequency. It shows that the modes of S2 have smoother envelopes and IF curves while those of S1 display oscillating signatures (e.g., see m2). These results provide

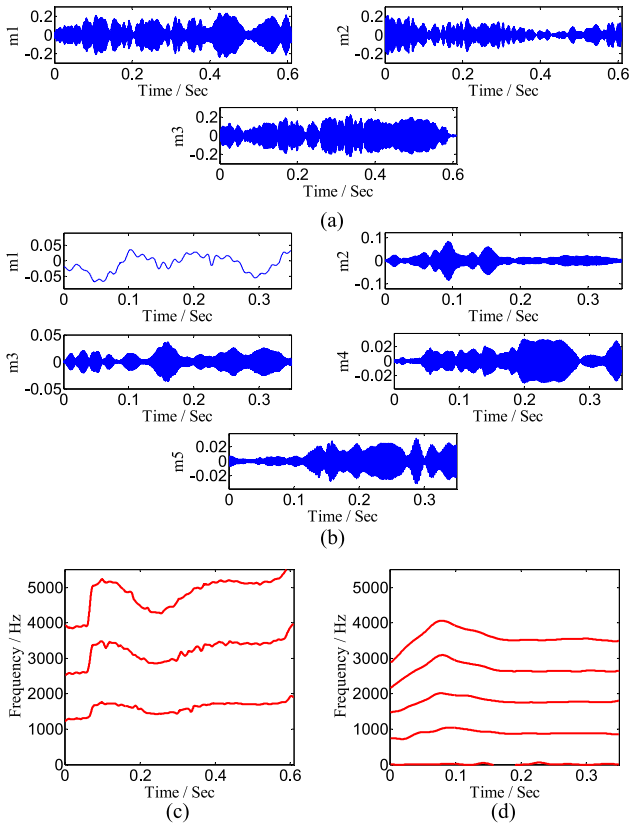

Fig. 13. Analysis results for the whale whistles. (a) Estimated modes for S1. (b) Estimated modes for S2. (c) Estimated IFs for S1. (d) Estimated IFs for S2.

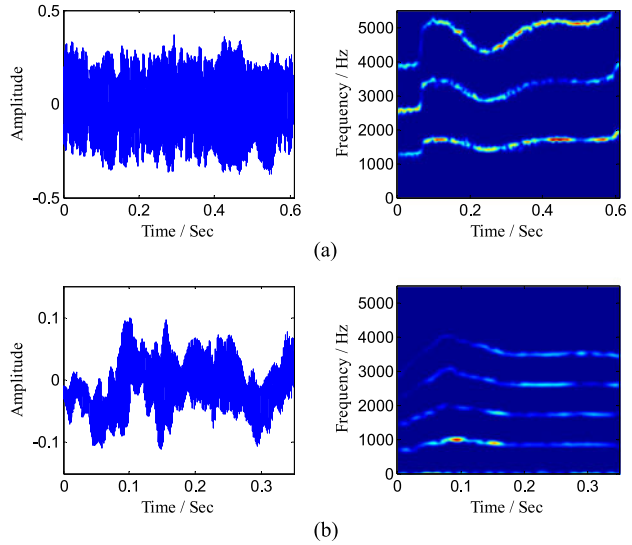

Fig. 14. Sum of the estimated modes. (a) S1. (b) S2.

valuable information for whale research. The sums of the estimated modes for S1 and S2 are illustrated in Fig. 14. By carefully comparing Figs. 12 and 14, we confirm that the VNCMD successfully recovers the signal features and significantly reduces the background noise. The two examples indicate the potential of our method in practical applications.

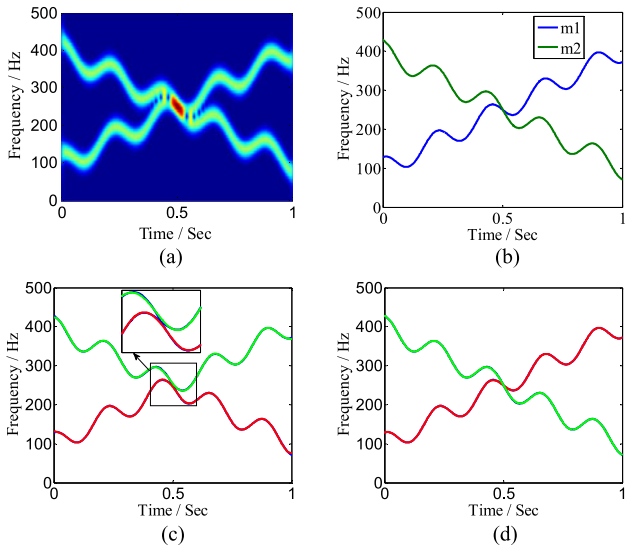

Fig. 15. Analysis results for the signal in (52) with different initial IFs by the VNCMD. (a) STFT of the signal. (b) True IFs of the signal. (c) Estimated IFs with constant initial IFs, i.e., 100 Hz for m1, 400 Hz for m2 (blue: true IFs; red: estimated IF for m1; green: estimated IF for m2). (d) Estimated IFs with linear initial IFs, i.e., 100+300t for m1, 400-300t for m2 (blue: true IFs; red: estimated IF for m1; green: estimated IF for m2).

C. Discussions

The preliminary results above show the potential of the VNCMD in analyzing signals containing close or even crossed modes, and also demonstrate its effectiveness in practical applications. However, it should be noted that (as mentioned in Section III-C) the convergence of the algorithm relies on the specified initial IFs. If the specified IFs are not that good, the algorithm may only find local minimums. In the simulations above, we simply choose some constant initial frequencies (e.g., the center frequencies of the modes for the example in (42)). However, in some complicated cases such as signals with severely crossed modes, a constant frequency may not always be a good initial guess for the time-varying IF of the target mode in the whole time span. Then, the results may become more like: in some time segments, the constant initial frequency is good enough for the method to find the correct mode; but, in other time segments, the method may find a wrong one since the same initialization may become too rough for the target mode. To show this limitation, we consider an example with two crossed chirps as:

$$\begin{aligned} g(t) &= g_{m1}(t) + g_{m2}(t) \\ &= \cos\left(2\pi\left(100t + 150t^2 + \sin(9\pi t)\right)\right) \\ &\quad + \cos\left(2\pi\left(400t - 150t^2 + \sin(9\pi t)\right)\right). \end{aligned} \tag{52}$$

The analysis results for this example with different initial IFs are shown in Fig. 15. Fig. 15(c) shows the estimated IFs of the method with constant initial IFs (i.e., 100 and 400 Hz for m1 and m2, respectively). It can be seen that the method tracks wrong modes after the intersection point (during 0.5 s $\sim$ 1 s). This is because that the constant frequencies are closer to the other modes after the intersection (i.e., the initial frequencies match with other modes better during 0.5 s $\sim$ 1 s). Even so, the two estimated IFs as a whole are almost coincident with the true IFs. This result indicates that the method has local properties and may track the local structures of other modes which are close to the specified initial IFs of the target modes. Therefore, for the signal with severely crossed modes, one should carefully choose the initial IFs according to the TF pattern of the considered signal. For example, if we choose linear initial IFs for the signal (52) (i.e., $100 + 300t$ and $400–300t$ for m1 and m2, respectively), the method will successfully catch the two modes as shown in Fig. 15(d). In more complicated cases, it may be difficult for users to empirically get good initializations. Fortunately, in those cases, we can follow the idea of some iterative TF methods such as the matching demodulation transform [35] which get initial IFs by detecting ridge curves from a TFR (e.g., the one by STFT). There are many methods available for ridge detection [29], [37], [49] some of which are effective for crossed signal modes (e.g., the improved Viterbi algorithm in [51]). The VNCMD can also be improved by using prior information on the signal model and imposing stronger regularity conditions on the IF model. For example, when dealing with the signals in (46) and (49), we can directly model the IF of the method as a polynomial, which will improve the convergence and the robustness of the method.

In addition, like some other decomposition methods such as the VMD [23], the EWT [22], and also some clustering algorithms, the number of the signal modes (i.e., Q in (15)) is assumed to be known in advance for the VNCMD. If we provide a wrong Q (i.e., fewer or more modes), imposing the strict constraint in (16) will be harmful to the convergence and may cause the stability issue of the algorithm (the influence is similar to that of specifying a very rough noise level σ as discussed in Section III-C). In this case, to alleviate the influence, we also choose to relax the constraint by dropping the Lagrangian multiplier λ and the noise variable w in (23) (e.g., see Fig. 4(b)). Then, in general, if we underestimate Q, we may only extract some of the modes by the method, and other modes will be totally discarded. In this case, the residual signal contains both the random noise and also deterministic signal modes. Therefore, we can identify this case by examining the property of the residue. On the other hand, if we overestimate the number of the modes, we may obtain some spurious modes which are mainly composed of noise. These modes usually exhibit poor energy concentration in a TFR, and show low correlation with the original signal. We can also identify this situation and then exclude the spurious modes in a post-processing step. In practice, one can also use some other methods to automatically estimate the number of modes in advance (e.g., the method in [49]).

V. Conclusion

In this paper, we presented a method (i.e., the VNCMD) to decompose a wide-band signal into a superposition of functions termed as NCMs. Based on the fact that a wide-band signal can be demodulated into a narrow-band signal, we formulated the decomposition as an optimal demodulation problem

in which the estimated modes should have the narrowest bands after being demodulated with the estimated IFs. One advantage of this formulation is that it does not rely on any parameterized model, which makes the method more adaptive to practical situations. Our optimization problem was efficiently solved by an improved ADMM approach which incorporates a restart scheme. We showed that the resulting algorithm have good convergence performance even in a noisy environment. To test the performance of the VNCMD, we first applied the method to analyze some artificial signals. The simulation results indicated that the method is more effective than the VMD and De-VSST in decomposing signals with close or even crossed modes. Finally, we presented an application of the method in analyzing whale whistles. Our future work will be devoted to improving the robustness of the method to the initializations when dealing with severely crossed modes and to the applications in various fields.

The code of the VNCMD is available on the Matlab Central website at http://cn.mathworks.com/matlabcentral/fileexchange/64292.

ACKNOWLEDGMENT

The authors would like to thank the editor and the reviewers for their valuable comments and suggestions which have significantly improved the manuscript.

REFERENCES

[1] B. Yang and M. Lugger, "Emotion recognition from speech signals using new harmony features," *Signal Process.*, vol. 90, no. 5, pp. 1415–1423, May 2010.

[2] B. Dugnol, C. Fernández, G. Galiano, and J. Velasco, "On a chirplet transform-based method applied to separating and counting wolf howls," *Signal Process.*, vol. 88, no. 7, pp. 1817–1826, Jul. 2008.

[3] L. Zuo, M. Li, X. Zhang, P. Zhang, and Y. Wu, "CFAR detection of range-spread targets based on the time-frequency decomposition feature of two adjacent returned signals," *IEEE Trans. Signal Process.*, vol. 61, no. 24, pp. 6307–6319, Dec. 2013.

[4] Z. Feng, M. Liang, and F. Chu, "Recent advances in time–frequency analysis methods for machinery fault diagnosis: A review with application examples," *Mech. Syst. Signal Process.*, vol. 38, no. 1, pp. 165–205, Jul. 2013.

[5] F. S. Cohen, S. Kadambe, and G. F. Boudreaux-Bartels, "Tracking of unknown nonstationary chirp signals using unsupervised clustering in the Wigner distribution space," *IEEE Trans. Signal Process.*, vol. 41, no. 11, pp. 3085–3101, Nov. 1993.

[6] N. E. Huang *et al.*, "The empirical mode decomposition and the Hilbert spectrum for nonlinear and non-stationary time series analysis," in *Proc. Royal Soc. A, Math., Phys. Eng. Sci.*, Mar. 1998, vol. 454, pp. 903–995.

[7] Y. Lei, J. Lin, Z. He, and M. J. Zuo, "A review on empirical mode decomposition in fault diagnosis of rotating machinery," *Mech. Syst. Signal Process.*, vol. 35, no. 1, pp. 108–126, Feb. 2013.

[8] H. Liang, Q.-H. Lin, and J. Chen, "Application of the empirical mode decomposition to the analysis of esophageal manometric data in gastroesophageal reflux disease," *IEEE Trans. Biomed. Eng.*, vol. 52, no. 10, pp. 1692–1701, Oct. 2005.

[9] M. K. I. Molla and K. Hirose, "Single-mixture audio source separation by subspace decomposition of hilbert spectrum," *IEEE Trans. Audio, Speech, Lang. Process.*, vol. 15, no. 3, pp. 893–900, Mar. 2007.

[10] F. Zhou, L. Yang, H. Zhou, and L. Yang, "Optimal averages for nonlinear signal decompositions—Another alternative for empirical mode decomposition," *Signal Process.*, vol. 121, pp. 17–29, Apr. 2016.

[11] N. Pustelnik, P. Borgnat, and P. Flandrin, "Empirical mode decomposition revisited by multicomponent non-smooth convex optimization," *Signal Process.*, vol. 102, pp. 313–331, Sep. 2014.

[12] T. Y. Hou and Z. Shi, "Adaptive data analysis via sparse time–frequency representation," *Adv. Adapt. Data Anal.*, vol. 3, no. 1, pp. 1–28, Apr. 2011.

[13] G. Rilling and P. Flandrin, "One or two frequencies? The empirical mode decomposition answers," *IEEE Trans. Signal Process.*, vol. 56, no. 1, pp. 85–95, Jan. 2008.

[14] Y. Qin, Y. Mao, and B. Tang, "Vibration signal component separation by iteratively using basis pursuit and its application in mechanical fault detection," *J. Sound Vib.*, vol. 332, no. 20, pp. 5217–5235, Sep. 2013.

[15] Z. Du, X. Chen, H. Zhang, and R. Yan, "Sparse feature identification based on union of redundant dictionary for wind turbine gearbox fault diagnosis," *IEEE Trans. Ind. Electron.*, vol. 62, no. 10, pp. 6594–6605, Oct. 2015.

[16] T. Y. Hou and Z. Shi, "Data-driven time–frequency analysis," *Appl. Computat. Harmon. Anal.*, vol. 35, no. 2, pp. 284–308, Sep. 2013.

[17] T. Y. Hou and Z. Shi, "Sparse time-frequency decomposition based on dictionary adaptation," *Philosoph. Trans. Roy. Soc. A*, vol. 374, no. 2065, Apr. 2016, Art. no. 20150192.

[18] A. Cicone, J. Liu, and H. Zhou, "Adaptive local iterative filtering for signal decomposition and instantaneous frequency analysis," *Appl. Computat. Harmon. Anal.*, vol. 41, no. 2, pp. 384–411, Sep. 2016.

[19] T. Qian, L. Zhang, and Z. Li, "Algorithm of adaptive fourier decomposition," *IEEE Trans. Signal Process.*, vol. 59, no. 12, pp. 5899–5906, Dec. 2011.

[20] R. R. Coifman, S. Steinerberger, and H. Wu, "Carrier frequencies, holomorphy and unwinding," 2016, arXiv:1606.06475.

[21] S. McNeill, "Decomposing a signal into short-time narrow-banded modes," *J. Sound Vib.*, vol. 373, pp. 325–339, Jul. 2016.

[22] J. Gilles, "Empirical wavelet transform," *IEEE Trans. Signal Process.*, vol. 61, no. 16, pp. 3999–4010, Aug. 2013.

[23] K. Dragomiretskiy and D. Zosso, "Variational mode decomposition," *IEEE Trans. Signal Process.*, vol. 62, no. 3, pp. 531–544, Feb. 2014.

[24] F. Auger and P. Flandrin, "Improving the readability of time-frequency and time-scale representations by the reassignment method," *IEEE Trans. Signal Process.*, vol. 43, no. 5, pp. 1068–1089, May 1995.

[25] F. Auger, E. Chassande-Mottin, and P. Flandrin, "Making reassignment adjustable: The levenberg-marquardt approach," in *Proc. IEEE Int. Conf. Acoust., Speech, Signal Process.*, 2012, pp. 3889–3892.

[26] I. Daubechies, J. Lu, and H.-T. Wu, "Synchrosqueezed wavelet transforms: An empirical mode decomposition-like tool," *Appl. Computat. Harmon. Anal.*, vol. 30, no. 2, pp. 243–261, Mar. 2011.

[27] T. Oberlin, S. Meignen, and V. Perrier, "Second-order synchrosqueezing transform or invertible reassignment? Towards ideal time-frequency representations," *IEEE Trans. Signal Process.*, vol. 63, no. 5, pp. 1335–1344, Mar. 2015.

[28] C. Y. Lin, L. Su, and H. Wu, "Wave-shape function analysis—When cepstrum meets time-frequency analysis," *J. Fourier Anal. Appl.*, 2017. [Online]. Available: https://doi.org/10.1007/s00041-017-9523-0

[29] D. Iatsenko, P. V. McClintock, and A. Stefanovska, "Nonlinear mode decomposition: A noise-robust, adaptive decomposition method," *Phys. Rev. E*, vol. 92, no. 3, Sep. 2015, Art. no. 032916.

[30] Y. Qin, B. Tang, and Y. Mao, "Adaptive signal decomposition based on wavelet ridge and its application," *Signal Process.*, vol. 120, pp. 480–494, Mar. 2016.

[31] S. Meignen, T. Oberlin, P. Depalle, P. Flandrin, and S. McLaughlin, "Adaptive multimode signal reconstruction from time–frequency representations," *Philosoph. Trans. Roy. Soc. A*, vol. 374, no. 2065, Apr. 2016, Art. no. 20150205.

[32] M. Kowalski, A. Meynard, and H.-T. Wu, "Convex optimization approach to signals with fast varying instantaneous frequency," *Appl. Computat. Harmon. Anal.*, 2016. [Online]. Available: https://doi.org/10.1016/j.acha.2016.03.008

[33] Y. C. Chen, M. Y. Cheng, and H. T. Wu, "Non-parametric and adaptive modelling of dynamic periodicity and trend with heteroscedastic and dependent errors," *J. Roy. Stat. Soc. B*, vol. 76, no. 3, pp. 651–682, Jun. 2014.

[34] J. R. Carson, "Notes on the theory of modulation," *Inst. Radio Eng.*, vol. 10, no. 1, pp. 57–64, Feb. 1922.

[35] S. Wang, X. Chen, G. Cai, B. Chen, X. Li, and Z. He, "Matching demodulation transform and synchrosqueezing in time–frequency analysis," *IEEE Trans. Signal Process.*, vol. 62, no. 1, pp. 69–84, Jan. 2014.

[36] B. Picinbono, "On instantaneous amplitude and phase of signals," *IEEE Trans. Signal Process.*, vol. 45, no. 3, pp. 552–560, Mar. 1997.

[37] S. Meignen, D.-H. Pham, and S. Mclaughlin, "On demodulation, ridge detection and synchrosqueezing for multicomponent signals," *IEEE Trans. Signal Process.*, vol. 65, no. 8, pp. 2093–2103, Apr. 2017.

[38] S. Chen, Y. Yang, K. Wei, X. Dong, Z. Peng, and W. Zhang, "Time-varying frequency-modulated component extraction based on parameterized demodulation and singular value decomposition," *IEEE Trans. Instrum. Meas.*, vol. 65, no. 2, pp. 276–285, Feb. 2016.
[39] Y. Yang, X. Dong, Z. Peng, W. Zhang, and G. Meng, "Component extraction for non-stationary multi-component signal using parameterized de-chirping and band-pass filter," *IEEE Signal Process. Lett.*, vol. 22, no. 9, pp. 1373–1377, Sep. 2015.
[40] Y. Yang, Z. Peng, X. Dong, W. Zhang, and G. Meng, "Application of parameterized time-frequency analysis on multicomponent frequency modulated signals," *IEEE Trans. Instrum. Meas.*, vol. 63, no. 12, pp. 3169–3180, Dec. 2014.
[41] M. C. Pan and Y. F. Lin, "Further exploration of vold–kalman-filtering order tracking with shaft-speed information—I: Theoretical part, numerical implementation and parameter investigations," *Mech. Syst. Signal Process.*, vol. 20, no. 5, pp. 1134–1154, Jul. 2006.
[42] S. Boyd, N. Parikh, E. Chu, B. Peleato, and J. Eckstein, "Distributed optimization and statistical learning via the alternating direction method of multipliers," *Found. Trends Mach. Learn.*, vol. 3, no. 1, pp. 1–122, Jan. 2011.
[43] N. Parikh and S. Boyd, "Proximal algorithms," *Found. Trends Optim.*, vol. 1, no. 3, pp. 127–239, 2013.
[44] M. Sadeghi and M. Babaie-Zadeh, "Iterative sparsification-projection (ISP): Fast and robust sparse signal approximation," *IEEE Trans. Signal Process.*, vol. 64, no. 21, pp. 5536–5548, Nov. 2016.
[45] J. Wang, X. Wang, L. Chen, J. Huangfu, C. Li, and L. Ran, "Noncontact distance and amplitude-independent vibration measurement based on an extended DACM algorithm," *IEEE Trans. Instrum. Meas.*, vol. 63, no. 1, pp. 145–153, Jan. 2014.
[46] B.-K. Park, O. Boric-Lubecke, and V. M. Lubecke, "Arctangent demodulation with DC offset compensation in quadrature doppler radar receiver systems," *IEEE Trans. Microw. Theory Techn.*, vol. 55, no. 5, pp. 1073–1079, May 2007.
[47] T. Goldstein, B. O'Donoghue, S. Setzer, and R. Baraniuk, "Fast alternating direction optimization methods," *SIAM J. Imag. Sci.*, vol. 7, no. 3, pp. 1588–1623, Aug. 2014.
[48] F. Millioz and N. Martin, "Circularity of the STFT and spectral kurtosis for time–frequency segmentation in white Gaussian environment," *IEEE Trans. Signal Process.*, vol. 59, no. 2, pp. 515–524, Feb. 2011.
[49] S. Meignen, T. Oberlin, and S. McLaughlin, "A new algorithm for multicomponent signals analysis based on synchrosqueezing: With an application to signal sampling and denoising," *IEEE Trans. Signal Process.*, vol. 60, no. 11, pp. 5787–5798, Nov. 2012.
[50] "Discovery of Sound in the Sea." 2002. [Online]. Available: http://www.dosits.org/
[51] H. Zhang, G. Bi, S. G. Razul, and C. M. S. See, "Robust time-varying filtering and separation of some nonstationary signals in low SNR environments," *Signal Process*., vol. 106, pp. 141–158, Jan. 2015.

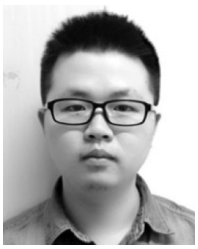

Shiqian Chen received the B.S. degree in mechanical engineering from Sichuan University, Chengdu, China, in 2014. He is currently working toward the Ph.D. degree in mechanical engineering at Shanghai Jiao Tong University, Shanghai, China.

He is currently with the State Key Laboratory of Mechanical System and Vibration, Shanghai Jiao Tong University. His current research interests include time–frequency analysis and machine health diagnosis.

Xingjian Dong received the B.S. degree in aircraft design engineering and the M.S. degree in solid mechanics from Northwestern Polytechnical University, Xi'an, China, in 1999 and 2002, respectively, and the Ph.D. degree in mechanical engineering from Shanghai Jiao Tong University, Shanghai, China, in 2006.

He is currently an Associate Professor with the State Key Laboratory of Mechanical System and Vibration, Shanghai Jiao Tong University. His current research interests include vibration analysis, smart structures, and fatigue analysis of structures.

Zhike Peng received the B.Sc. and Ph.D. degrees from Tsinghua University, Beijing, China, in 1998 and 2002, respectively.

He was a Research Associate at the City University of Hong Kong, Hong Kong, from 2003 to 2004, and a Research Officer with Cranfield University, Cranfield, U.K. He was at the University of Sheffield, Sheffield, U.K., for four years. He is currently a Cheung Kong Chair Professor with the State Key Laboratory of Mechanical System and Vibration, Shanghai Jiao Tong University, Shanghai, China. His current research interests include nonlinear vibration, signal processing and condition monitoring, and fault diagnosis for machines and structures.

Wenming Zhang (M'10) received the B.S. degree in mechanical engineering and the M.S. degree in mechanical design and theories from Southern Yangtze University, Wuxi, China, in 2000 and 2003, respectively, and the Ph.D. degree in mechanical engineering from Shanghai Jiao Tong University, Shanghai, China, in 2006.

He is currently a Professor with the State Key Laboratory of Mechanical System and Vibration, School of Mechanical Engineering, Shanghai Jiao Tong University. He has been working in the dynamics and control for micro/nanoelectromechanical systems (MEMS/NEMS). His current research interests include nonlinear dynamics and chaos control, nonlinear vibration and control, coupled parametrically excited microresonators, and the reliability analysis and assessment for MEMS/NEMS applications.

Guang Meng received the Ph.D. degree from Northwestern Polytechnical University, Xi'an, China, in 1988.

He is currently a Professor of the State Key Laboratory of Mechanical System and Vibration, Shanghai Jiao Tong University, Shanghai, China. In 1993, he was a Professor and the Director of Vibration Engineering Institute with Northwestern Polytechnical University. From 1989 to 1993, he was also a Research Assistant with Texas A&M University, College Station, TX, USA, an Alexander von Humboldt Fellow with Technical University Berlin, Berlin, Germany, and a Research Fellow with New South Wales University, Sydney, NSW, Australia. From 2000 to 2008, he was with Shanghai Jiao Tong University, as the Cheung Kong Chair Professor, the Associate Dean, and the Dean of the School of Mechanical Engineering. His research interests include dynamics and vibration control of mechanical systems, nonlinear vibration, and microelectromechanical systems.